https://doi.org/10.5194/egusphere-2023-285
Preprint. Discussion started: 7 March 2023
© Author(s) 2023. CC BY 4.0 License.

Aeolus wind lidar observations of the 2019/2020 Quasi-Biennial Oscillation disruption with comparison to radiosondes and reanalysis

Timothy P. Banyard[1], Corwin J. Wright[1], Scott M. Osprey[2, 3], Neil P. Hindley[1], Gemma Halloran[4], Lawrence Coy[5, 6], Paul A. Newman[5], and Neal Butchart[7]

[1]Centre for Space, Atmospheric and Oceanic Science, University of Bath, Bath, UK
[2]National Centre for Atmospheric Science, Oxford, UK
[3]Department of Physics, University of Oxford, Oxford, UK
[4]Met Office, Exeter, UK
[5]NASA Goddard Space Flight Center Greenbelt, Maryland, USA
[6]SSAI, Lanham, Maryland, USA
[7]Met Office Hadley Centre, Reading, UK

Correspondence: Timothy P. Banyard (tpb38@bath.ac.uk)

Abstract. The quasi-biennial oscillation (QBO) was unexpectedly disrupted for only the second time in the historical record during the 2019/20 boreal winter. As the dominant mode of atmospheric variability in the tropical stratosphere, and a significant source of seasonal predictability globally, understanding the drivers behind this unusual behaviour is very important. Here, novel data from Aeolus, the first Doppler wind lidar in space, is used to observe the 2019/20 QBO disruption. Aeolus is the first satellite able to observe winds at high resolution on a global scale, and is therefore a uniquely capable platform for studying the evolution of the disruption and the broader circulation changes triggered by it. This study therefore contains the first direct wind observations of the QBO from space, and exploits measurements from a special Aeolus scanning mode, implemented to observe this disruption as it happened. Aeolus observes easterly winds of up to 20 ms^{-1} in the core of the disruption jet during July 2020. By co-locating with radiosonde measurements from Singapore and ERA5 reanalysis, like-for-like comparisons of the observed wind structures in the tropical stratosphere are produced, showing equatorial Kelvin wave activity and key parts of the Walker Circulation during the disruption period. The onset of the disruption easterly jet occurs 5 days earlier in Aeolus observations compared with the reanalysis. This analysis highlights how Aeolus and future Doppler wind lidar satellites can deepen our understanding of the QBO, its disruptions, and the tropical upper-troposphere lower-stratosphere region more generally.

1 Introduction

The Quasi-Biennial Oscillation (QBO) is a regular cycle of alternating, downward propagating westerly and easterly winds which dominates the behaviour of the tropical stratosphere (Wallace, 1973). Observed continuously since 1953 using radiosonde measurements (Naujokat, 1986), the QBO has a relatively predictable period of 28±4 months with a typical maximum amplitude between 20-30 ms^{-1} (Bushell et al., 2020). In addition to its impact on the tropical tropopause, and therefore

https://doi.org/10.5194/egusphere-2023-285
Preprint. Discussion started: 7 March 2023
© Author(s) 2023. CC BY 4.0 License.

convection and related phenomena such as the Madden-Julian Oscillation (Feng and Lin, 2019; Lim et al., 2019), the QBO has also been shown to modulate the atmospheric circulation in the extratropical regions, and is an important source of predictability globally (Scaife et al., 2014). Furthermore, given that it is primarily a wind-based phenomenon, any new methods of measuring wind in this region of the atmosphere present a good opportunity to study the QBO from a completely different perspective.

Launched in September 2018, Aeolus is the first wind lidar in space. It is capable of measuring winds at high vertical resolution almost globally in the lowermost 30 km of the atmosphere, and thus theoretically the lower portion of the QBO. Since the QBO is highly technically challenging to model, wind observations are vital to understand it fully. Aeolus therefore presents a novel opportunity to measure the QBO directly and in its full zonal extent for the first time. To realise this potential, a special campaign involving a change to the satellite's onboard settings was initiated, raising the highest measuring altitude to observe a greater depth of the QBO.

Despite the remarkable consistency of the QBO since 1953, since 2016 there have been two major and unprecedented disruptions to its expected evolution. The first, beginning in late 2015, was almost certainly caused by extratropical Rossby wave propagation during the Northern Hemisphere winter; and has already been studied extensively (e.g. Osprey et al., 2016; Newman et al., 2016; Coy et al., 2017; Barton and McCormack, 2017; Kang et al., 2020, and others). The second began in late 2019, and it has been proposed that anomalous Rossby wave activity from the Southern Hemisphere was partly responsible for this event (Kang and Chun, 2021). Irrespective of their causal mechanisms, neither disruption was well predicted by forecast models, and the possibility of a link to anthropogenic climate change (Anstey et al., 2021) in addition to the high possible impact on future predictability, necessitates a more robust explanation for the dynamical processes which drive such phenomena.

This study explores the evolution of the 2019-2020 QBO disruption using measurements from Aeolus. Section 2 outlines the methods involved in this study, with a description of the data used from Aeolus, ERA5 reanalysis and Singapore radiosondes. Section 3 shows the evolution of the disruption from multiple angles, including a validation of the data used and a look at the equatorial waves involved. Section 4 offers a discussion of this study's limitations and a summary of the key points for future work. Section 5 concludes this paper with an outline of its main findings.

2 Data and Methods

In this study, the 2019-2020 QBO disruption is observed using data from a tropical rawinsonde station at Singapore, the Aeolus wind lidar satellite, and the ERA5 reanalysis. These give a local, global and reanalysis perspective of the disruption, thus providing complimentary measurements of its evolution. In this section, each of the datasets is introduced, as well as the procedures followed to provide an appropriate comparison between them. Also explored are the methods used to best highlight the QBO's important characteristics, and the details of the analytical techniques used to deconstruct the causes and effects of the disruption itself.

https://doi.org/10.5194/egusphere-2023-285
Preprint. Discussion started: 7 March 2023
© Author(s) 2023. CC BY 4.0 License.

2.1 Singapore Radiosonde

The tropical rawinsonde station at Singapore (1°N, 104°E) produces twice-daily high-resolution meteorological soundings which are stored as part of the Integrated Global Radiosonde Archive (Durre et al., 2018). For the majority of the time period covered in this analysis, this station used the Vaisala VRS41-SG radiosonde (Vaisala, 2014) and Vaisala DigiCORA III sounding system to receive and process wind information, giving values for the wind speed and direction with an uncertainty of 0.15 ms^{-1} and 2° respectively. Each radiosonde reaches a typical altitude of around 30 - 35 km and provides data at a mean vertical resolution of 250 m. Due to the weekly recurrence of a special setting onboard Aeolus for measuring the QBO, designed to coincide with one of the closest overpasses with an average minimum proximity to the rawinsonde station of ∼80 km, only the 00:00 UTC sounding from Singapore on a Thursday is used. Realistic comparisons with Aeolus winds are obtained by projecting the radiosonde winds onto the same direction as the Aeolus measurement geometry. Although the geographical discrepancy between the two datasets is not negligible, its effect on the results are not deemed significant given the context of the QBO, which is a large-scale atmospheric phenomenon. Data used in this study covers the time period from early-2019 to late-2021.

2.2 Aeolus

Aeolus is a satellite launched in August 2018 carrying the first space-borne wind lidar instrument, called the Atmospheric Laser Doppler Instrument (ALADIN) (ESA, 1989, 2008; Chanin et al., 1989; Stoffelen et al., 2005; Reitebuch, 2012). As described by Banyard et al. (2021), its mission is to provide high vertical resolution profiles of wind, aerosol and cloud along its orbital path, with near global coverage. Observations are made by measuring backscattering from atmospheric molecules (Rayleigh scattering), and aerosol and hydrometeors (Mie scattering) along the laser's line-of-sight (LOS). Typically, the instrument measures from the surface up to around 20 km, however special configurations have enabled measurements to be made up to 30 km in specific regions and at certain times (Legras et al., 2022).

The satellite's orbit is sun-synchronous with 15.6 orbits each day and a repeat cycle of 7 days, and for the duration of the observing period in this study there is a close overpass to the site of the Singapore rawinsonde station between 22:55 and 23:00 UTC every Wednesday. Aeolus' orbit has an inclination of 96.97°, resulting in a near-meridional orbital path at the equator, and it flies at a mean altitude of 320 km, with an ascending-node local equator-crossing time of 18:00.

To enable the instrument to provide an observation of the horizontal wind, both laser and telescope are directed at 35° off-nadir, perpendicular to the direction of travel. This is particularly advantageous for observing the QBO, since Aeolus wind measurements are inherently near-zonal in the tropical lower-stratosphere. Along the LOS of the laser a single wind component is measured, which is then converted into the horizontal line-of-sight (HLOS) wind speed v_{HLOS} through the assumption that the vertical wind speed is small. Equations describing Aeolus' measurement geometry can be found in Banyard et al. (2021), and a more detailed description and exploration of its limitations is in Krisch et al. (2022).

Raw Aeolus observations are processed to produce measurements of the HLOS wind speed and placed in 24 vertical "range bins", each with thicknesses between 250 and 2,000 m, which can be modified by the satellite operators. Numerical Weather

https://doi.org/10.5194/egusphere-2023-285
Preprint. Discussion started: 7 March 2023
© Author(s) 2023. CC BY 4.0 License.

Prediction (NWP) requirements are such that the vertical resolution of Aeolus wind data is around ∼1 km in the UTLS region, with this tending towards 2 km in the lower stratosphere. This inevitably means the data is relatively coarse in the region of the QBO, and therefore at the altitude of the 2019-2020 disruption. To better observe the evolution of the QBO following this event, a special range-bin setting (RBS) was implemented onboard the spacecraft (see figure 1) beginning in June 2020. This raised the maximum altitude of each wind profile by 5000 m to 25.5 km in the latitude range 10°S - 10°N each Wednesday. Bins lower down were also modified to maintain an appropriate bin spacing throughout the atmospheric profile. Since the QBO varies over a long temporal scale, the implementation of this RBS once per week is sufficient to provide suitable information about the QBO's evolution in the lower stratosphere.

In this study, the most recently available Level 2B (L2B) product for each time is used, ranging progressively from processing Baseline 11 to Baseline 14, which includes some reprocessed data for certain periods during the mission. Quality controls are applied, including a restriction to only use Rayleigh clear observations, which maximises data coverage while preserving data quality, and an 8 ms^{-1} cut off on the random error for each data point. Recent literature shows systematic biases of <1ms^{-1} for the Rayleigh wind L2B product (Abdalla et al., 2020), suggesting the dominant source of error is the random error of the instrument. This is alleviated somewhat where a daily zonal-mean wind is calculated, due to the large number of data points that are included.

Since the QBO is a phenomenon defined by the zonal component of the wind, it is desirable to extract this component from the original HLOS product provided by Aeolus. A number of methods can be implemented to achieve this, as discussed by (Krisch et al., 2022). Here, the third method from that work is used, since it produces the best results with the least systematic error, is suitable in the band 60°S - 60°N, and is primarily limited by its spatiotemporal constraints, for which analysis of the QBO is generous.

2.3 ERA5

ERA5 is an atmospheric reanalysis data set provided by the ECMWF. It is a combination of an earth-system model with assimilated observations which supplies a historical archive of the atmospheric state globally (Hersbach et al., 2020). ERA5 has a spatial resolution of 0.25°×0.25° (∼31 km), 137 vertical levels from the surface up to 0.1 hPa, and the data-set used here has a temporal resolution of three hours. For the purposes of this study, ERA5 data has been projected onto the Aeolus HLOS for each data point to create a matching dataset which simulates Aeolus orbiting through an ERA5-like atmosphere. This allows the same analysis to be conducted on both Aeolus and ERA5 data to give appropriate comparisons between the two. Although Aeolus data is not assimilated into ERA5, observations from the Singapore radiosonde are, which is an important factor to consider during the subsequent comparisons.

https://doi.org/10.5194/egusphere-2023-285
Preprint. Discussion started: 7 March 2023
© Author(s) 2023. CC BY 4.0 License.

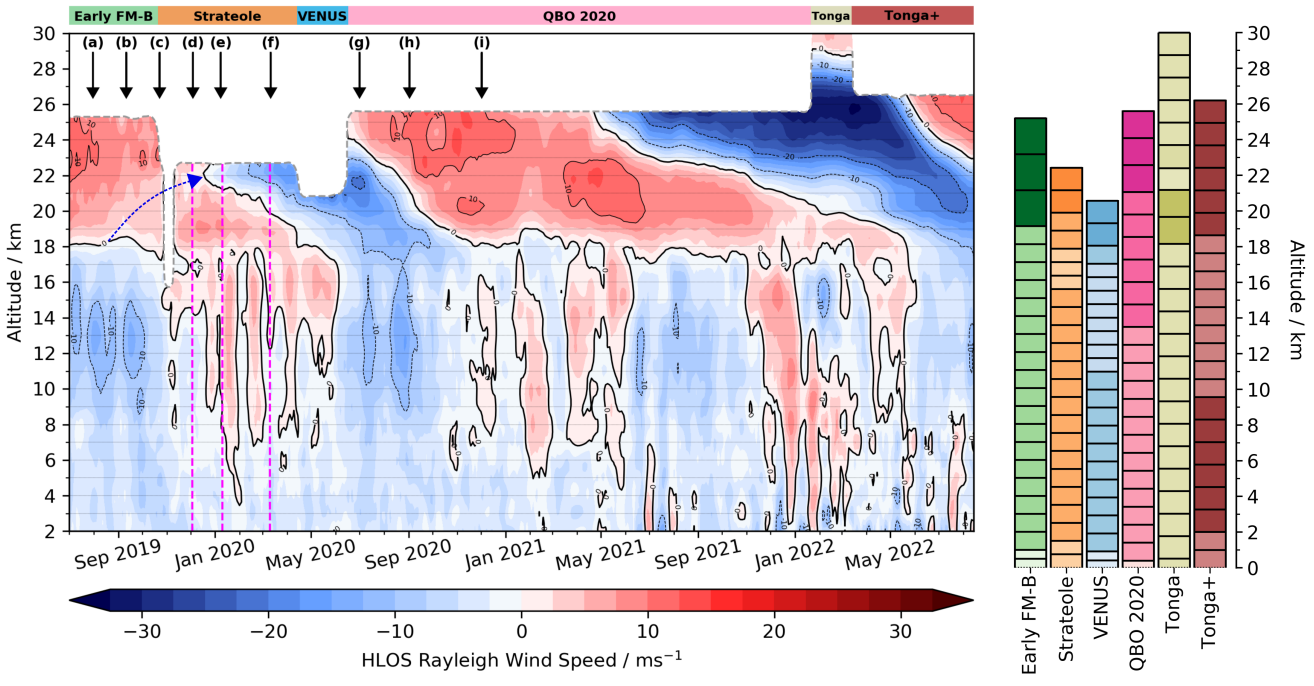

Figure 1. Timeseries of daily zonal-mean HLOS wind from Aeolus between 5°S - 5°N. The grey dashed line signifies the altitude of the highest range-bin observed at that time. This altitude varies according to a series of successive RBS changes, which are illustrated with a bar plot on the right hand side of the figure, with lighter shades denoting shallower bins. The duration of each respective RBS for this latitudinal range is shown by coloured bars above the time series. The 9 black arrows shown just underneath correspond to the dates of the profile comparisons shown in figure 3(a-i). The dashed blue arrow marks the ascending region of suppressed westerlies which precedes the disruption. The 3 dashed magenta lines during the period of the disruption correspond to the cross-sectional snapshots in figure 7.

3 Results

3.1 Aeolus observations of the QBO disruption

Both QBO disruptions were characterised by the stalling of the normal descent of the zonal wind bands in the tropical stratosphere and the formation of a second anomalous easterly layer within the lower stratospheric westerly QBO phase. Figure 1 portrays the evolution of the 2019-2020 QBO disruption, and the subsequent QBO cycle, as observed by Aeolus. The initial disruption at the end of 2019 is followed in late 2020 and 2021 by the resumption of the descent of the active westerly phase of the QBO, with the next QBO cycle appearing towards the end of the time series.

Only the lowermost portion of the QBO is observed by Aeolus due to the constraints imposed by the RBS, but nonetheless, the beginning of the wind reversal to easterlies can be seen clearly during December 2019 at 22 km. This is preceded by a

https://doi.org/10.5194/egusphere-2023-285
Preprint. Discussion started: 7 March 2023
© Author(s) 2023. CC BY 4.0 License.

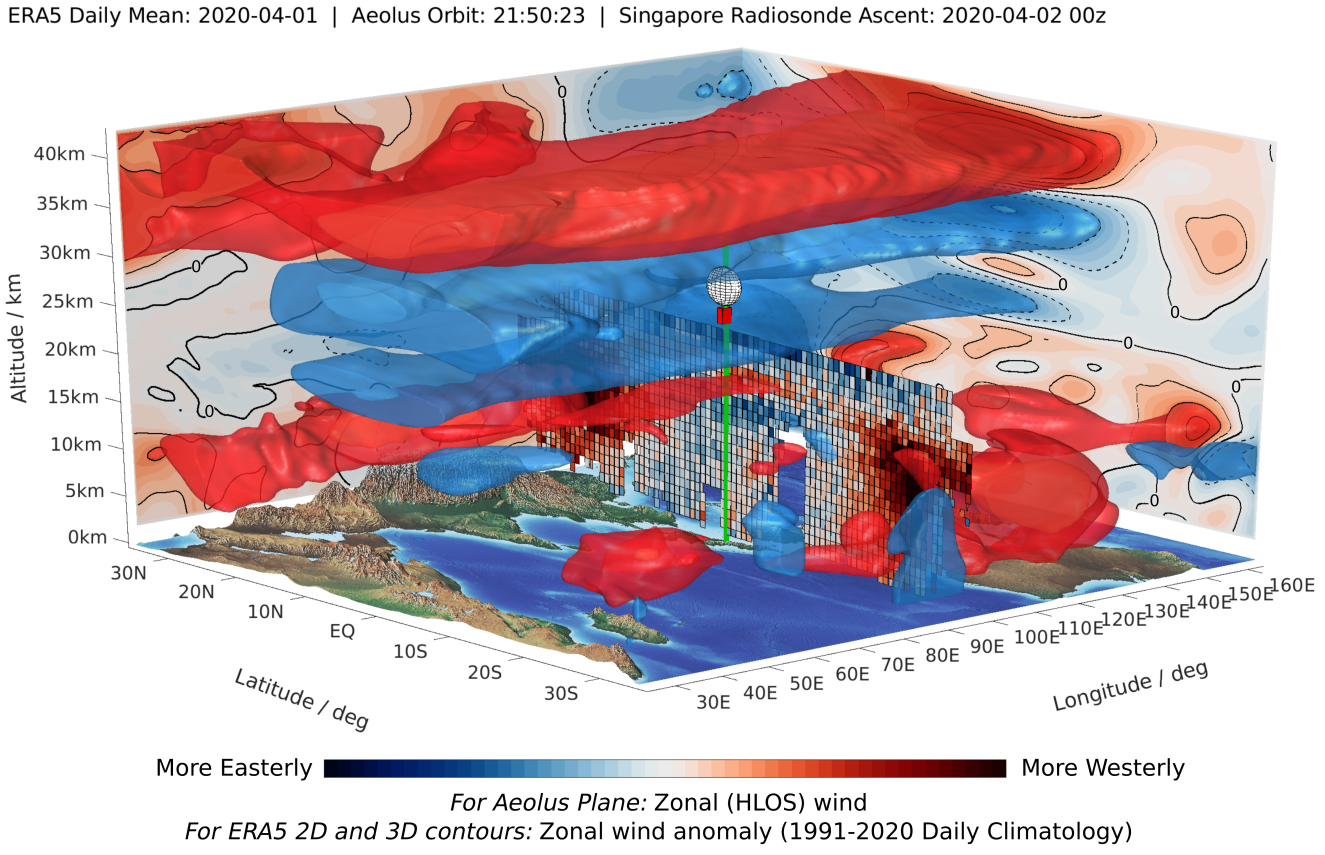

Figure 2. Illustration of the three datasets used in this study and the manner in which they relate to each other. ERA5 zonal wind anomalies are shown using coloured contours, with 3D contours at -22, -11, 11 and 22 m/s to highlight the important features of the QBO disruption. Along-track profiles of Aeolus data and the launch trajectory of the Singapore Radiosonde are also shown, with the exact location of each data point used for both data sets. This figure is intended to give a qualitative perspective which helps the reader understand the broader context behind the data which gives the results in this paper.

https://doi.org/10.5194/egusphere-2023-285
Preprint. Discussion started: 7 March 2023
© Author(s) 2023. CC BY 4.0 License.

narrow, ascending region of suppressed westerlies, emanating from near the tropopause during August-September 2019, which is marked by the dashed blue arrow.

Following the wind reversal, the region of disruption easterlies expands vertically with time, with the lower wind-shear zone progressing downwards in a QBO-like manner. In July 2020 this easterly jet reaches a maximum magnitude of 20 ms^{-1} at 22 km, although this measurement is hindered by the RBS at the time. The new RBS then reveal the now downward-propagating upper wind-shear zone in mid-2020, as westerly winds quickly follow the disruptive easterlies. Later in 2021, the highest range-bins begin to show the subsequent easterly QBO phase, which progresses uninterrupted through to nearly the end of the data period. During 2022, new RBS to measure the volcanic plume from the eruption of the Hunga-Tonga volcano are introduced, revealing the next westerly phase of the QBO, which descends from the top range-bin of 30 km to around 23 km by the end of the period.

Throughout much of the time-series, a series of westerly wind pulses can be seen in the middle- and upper-troposphere, in the midst of more persistent easterly winds which dominate the tropical troposphere. The temporal frequency of these pulses suggests the occurrence of significant tropical wave activity, likely related to Kelvin waves, particularly during the evolution of the disruption following its triggering in late-2019. Further analysis on the propagation of these waves along the equator is carried out later in this study, and three representative snapshots of their vertical structure, corresponding to the times marked by the magenta dashed lines, will be considered in section 3.3.

These pulses of westerly winds exhibit a seasonality which can likely be explained by phenomena called westerly wind bursts (WWBs), which are thought to play an important role in the initiation of El Nino events. Driven at least in part by atmospheric Kelvin waves, Pacific-basin WWBs induce anomalous ocean surface wind stresses and initiate oceanic Kelvin wave propagation through the equatorial Pacific, deepening the thermocline and accelerating the onset of El Nino conditions (Tan et al., 2020). As noted by Seiki and Takayabu (2007), WWBs appear to be more common between November and April, matching the stronger westerly winds seen in figure 1 during the boreal winters of 2019-20, 2020-21 and 2021-22. Some literature has discussed the presence of a so-called 'spring predictability barrier' which causes El Nino forecasts to rapidly increase in skill with decreasing lead-time throughout the boreal spring period (Latif et al., 1998; Zheng and Zhu, 2010; Chen et al., 2020). Its timing is often linked with the occurrence of such WWBs due to the oceanic processes that are triggered. More accurate measurements of WWBs provided by space-borne wind lidars such as Aeolus could therefore prove useful in combatting predictability issues such as this.

The fine vertical resolution of Aeolus data in the UTLS allows the behaviour of winds in the vicinity of the tropopause to be observed in detail. Due to the strong turbulence and vertical winds that distinguish the troposphere from the stratosphere, the QBO does not extend below the tropopause, although some previous studies have observed a weak oscillation comparable to the QBO at the tropopause itself (Angell and Korshover, 1964; Reid and Gage, 1985). The tropopause is a boundary most often defined by the altitude at which the vertical gradient in temperature reverses, commonly known as the cold point tropopause (CPT) (Highwood and Hoskins, 1998). Since the QBO is a wind phenomena however, it is useful to understand the lower limit of its downward propagation from a wind based perspective. Using GNSS-RO data, Tegtmeier et al. (2020) showed that the amplitude of the QBO at the CPT varies with longitude, and there is uncertainty about both the spatial and temporal variability

https://doi.org/10.5194/egusphere-2023-285
Preprint. Discussion started: 7 March 2023
© Author(s) 2023. CC BY 4.0 License.

of the QBO's vertical extent. In the timeseries in figure 1, the lower limit of the QBO in a zonal-mean framework remains steady between around 17 and 18 km, around a kilometre above the typical tropopause altitude between 5°N and 5°S.

Since the tropical tropopause layer (TTL) is a region where important transfers of energy, chemical species and water vapour occur, the addition of high vertical resolution wind measurements from Aeolus and similar wind lidars is desirable, particularly for assimilation into atmospheric reanalyses. Currently, radiosonde analyses form much of our understanding about TTL processes, particularly since these pre-date the satellite era and give a longer historical record. Later in this study, 9 radiosonde profiles from Singapore are compared with ERA5 and Aeolus; the timings of these during the QBO disruption are denoted with arrows which are marked (a) to (i) in figure 1.

To the right of the timeseries in figure 1 are six stacked bar charts showing the different RBS that are active throughout the measurement period, illustrating the importance of the QBO 2020 RBS for observing the QBO disruption and its subsequent evolution, with an increase in the top altitude of ∼5 km. In 2022, a further increase to the highest altitude of Aeolus data can be seen, corresponding to the introduction of new RBS to observe the stratospheric effects of the Tonga eruption of 15 January 2022. One of the unintended consequences of this change is observations of the QBO up to 30 km using Aeolus for the first time, allowing the initial signs of westerly winds associated with the next QBO phase to be observed above ∼28 km. Despite the decreased signal-to-noise ratio (SNR) at these heights, the large number of data points (up to ∼200) being used for a zonal-mean daily wind value between 5°N and 5°S means that this is likely to still be a trustworthy result. Since much of the dynamical forcing associated with the QBO takes place at such altitudes, wind measurements here by future Doppler wind lidar (DWL) satellites could prove very useful, both for deepening scientific understanding and improving model predictions of the QBO.

3.2 Validation against reanalysis and radiosondes

In order to validate the data from Aeolus as the disruption evolves, co-located ERA5 reanalysis and high altitude radiosonde launches from Singapore are used. Figure 2 illustrates these three datasets in relation to each other, showing the location of the radiosonde launch site and the closest intersecting Aeolus orbit, as well as the context of the ERA5 zonal wind anomaly at the time of the disruption itself. The back plane of the figure shows an equatorial cross-section of the zonal wind near 160°E, from ERA5, which matches up with the 3D contours plotted throughout the image.

Clear spatial and temporal limitations of the comparison between the datasets are seen, with the almost fixed horizontal location of the radiosonde and the single descending-node Aeolus orbit used being particularly notable. Radiosonde data from Singapore is used partly due to the good continuity of its record; indeed data from this station is often used as a proxy for the QBO's historical progression. Conversely, as in Kawatani et al. (2016), it is possible that radiosonde data strongly constrains the reanalysis towards itself. This leads to the higher variability of winds across different reanalyses in data sparse regions, such as over the Pacific ocean, where each reanalysis will drift towards the model's climatology. Such a dependence is important to remember throughout this analysis.

In figure 2, the disruption easterly and underlying westerlies can be seen clearly in the ERA5 zonal wind anomaly and Aeolus overpass. Also notable is the widening in latitudinal extent of the QBO and disruption anomalies with increasing altitude, all

https://doi.org/10.5194/egusphere-2023-285
Preprint. Discussion started: 7 March 2023
© Author(s) 2023. CC BY 4.0 License.

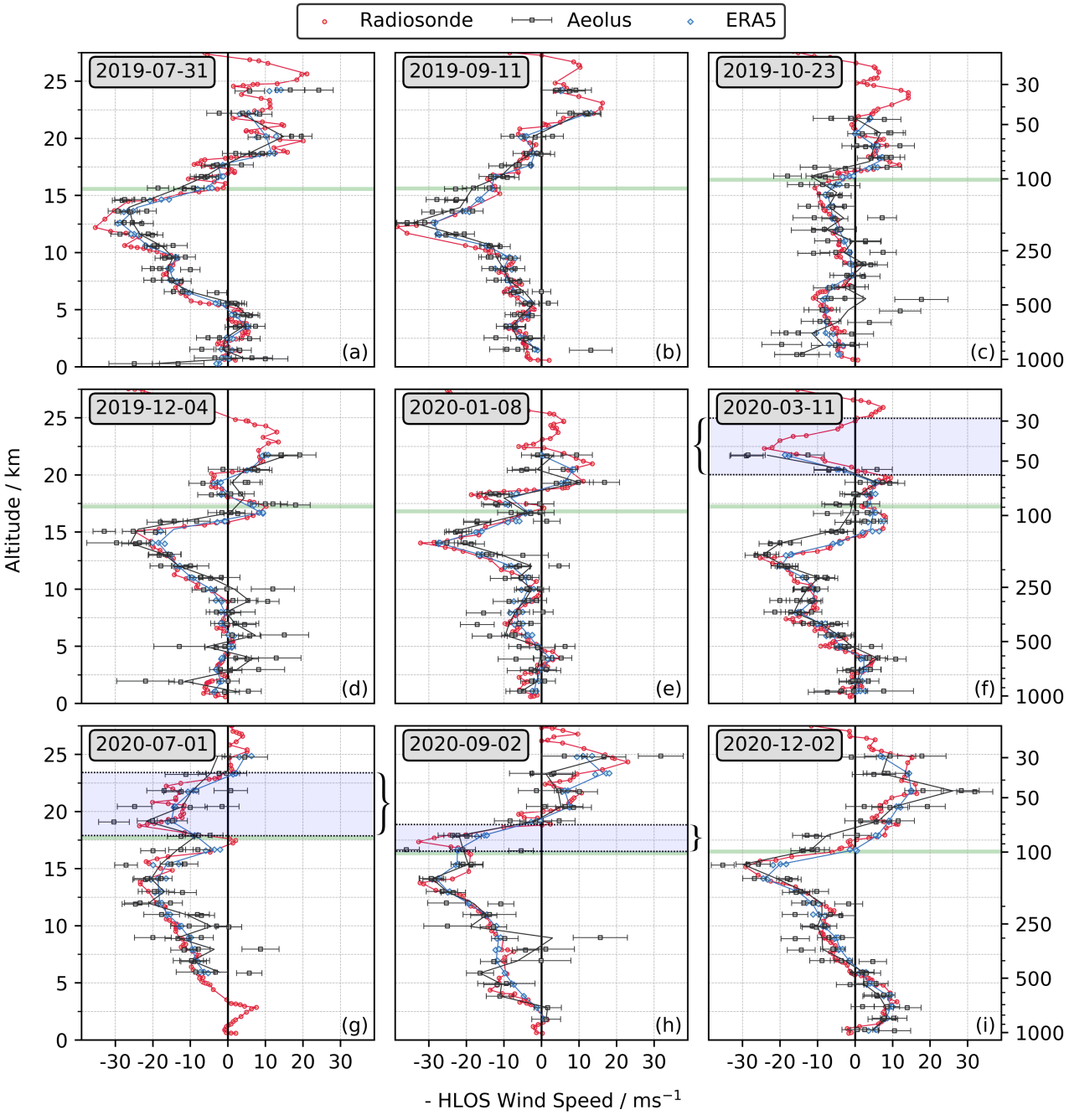

Figure 3. (a)-(i) Profiles of the HLOS wind from Aeolus (black), projected-HLOS wind from ERA5 (blue) and projected-HLOS wind from Singapore-launched radiosondes (red) for a progression of time-steps during the QBO disruption. Lines follow the average of profiles within the 250 km radius surrounding area at each range-bin height for Aeolus and ERA5. Error bars shown for Aeolus correspond to the HLOS error estimates given in the L2B files. The ERA5 tropopause for each day is shown by a horizontal green line, and the easterly disruption region above the tropopause is marked by the pale blue region bounded by curly brackets. The corresponding timestamp is shown in the top-left corner of each subplot.

https://doi.org/10.5194/egusphere-2023-285
Preprint. Discussion started: 7 March 2023
© Author(s) 2023. CC BY 4.0 License.

the way up to 40 km, a property of the QBO which is observed in previous literature (Reed, 1965). The subtropical jet streams can also be observed in this figure, and are shown for completeness.

The perspective given by the 3D along-track profiles of Aeolus also demonstrates the acute angle that the satellite's orbit follows relative to the meridian, which leads to the Aeolus HLOS winds being very representative of the zonal wind, as the ALADIN laser is directed perpendicular to the direction of travel. On close inspection, the latitudinal limits of the VENUS equatorial RBS, 30°S-30°N, which existed prior to the QBO 2020 RBS, can be seen. Both subtropical jets in the northern and southern hemispheres, present during April 2020, can also be clearly seen polewards of 20°S and 20°N. Gaps in the Aeolus data are also visible, particular where there are more convective clouds such as in the intertropical convergence zone (ITCZ). One limitation of using just the Rayleigh clear Aeolus HLOS winds is that cloudy returns are removed by quality control, so the winds within the ITCZ are likely to be represented less well in this data.

A set of nine Aeolus overpasses, each overlaid with the corresponding Singapore radiosonde profile and ERA5 data for the same time, is shown in figure 3. Only Aeolus profiles within 250 km of the Singapore launch site are used since the larger-scale dynamics should not change significantly across this area; this also accounts for drift in the radiosonde location as it ascends. Since reprocessed Aeolus data is being used, any systematic biases that arise from using solely descending node overpasses should be kept to a minimum (Weiler et al., 2021). In order to match the zonal wind speed direction, all Aeolus winds are sign-flipped on the descending node to become -HLOS, i.e. negative HLOS. This is required because ALADIN's laser is directed perpendicularly to the right hand side of the satellite's orbital path. The error in the Singapore radiosonde measurements and ERA5 projected-HLOS is considered small relative to the given HLOS error from Aeolus. From (a-i), each set of profiles shows a representative snapshot throughout the disruption period. Dates are chosen to give a good representation of the entire disruption, from its initiation, to its evolution and after-effects, and only where good-quality data is available from all datasets.

Good agreement between all three datasets is seen throughout, with the same persistent easterly winds which are seen dominating the tropical troposphere in figure 1, clearly shown. In figure 3f, the disruption easterly is clearly discernible in all three datasets, with local easterly winds reaching 20 m/s in mid-March around 22 km, this region has deepened and descended slightly by early-July (figure 3g) such that only a thin sliver of westerly winds can be seen in the radiosonde data around the altitude of the tropopause. By the end of 2020 (figure 3i), the westerly QBO has descended through the lower stratosphere, although the altitude of the zero-wind zone is around 2 km higher in Aeolus compared with the radiosonde and ERA5. A similar discrepancy can be seen during mid-March (figure 3f), with Aeolus observing winds around 14 km that are up to 15 m/s more easterly than the comparison datasets. The absence of Aeolus winds below 5 km in figure 3g is most likely due to cloud in the lower troposphere, and the slightly higher random error throughout the atmospheric profile in this and the profile in figure 3h could be attributed to cloud contamination in the backscattered Rayleigh signal.

By combining all available profiles from each Wednesday during the time period, selected to correspond with the day the QBO 2020 RBS is active, figure 4 shows distributions of the differences between the 3 datasets for (a) Aeolus - Singapore Radiosonde, (b) Aeolus - ERA5 and (c) Singapore Radiosonde - ERA5. Since the radiosonde data is assimilated into ERA5, the significantly lower difference between these two datasets (figure 4c) is to be expected. Once again, good agreement between all three datasets is seen, with median differences of -0.44 ms^{-1} and 0.15 ms^{-1} between Aeolus, and the Singapore Radiosonde

https://doi.org/10.5194/egusphere-2023-285
Preprint. Discussion started: 7 March 2023
© Author(s) 2023. CC BY 4.0 License.

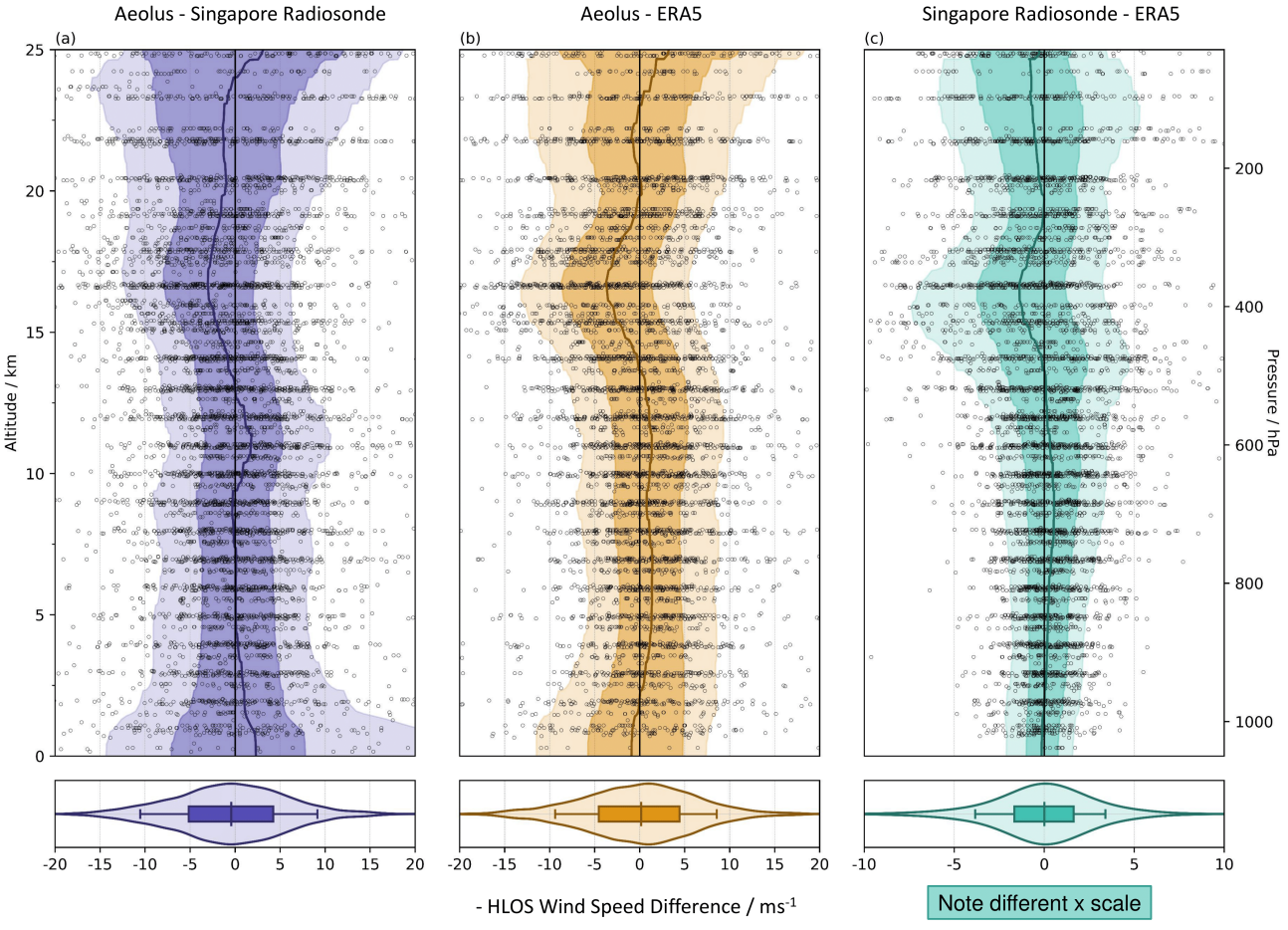

Figure 4. Vertical distribution of the point-by-point HLOS wind speed difference for (a) Aeolus-Singapore, (b) Aeolus-ERA5, (c) ERA5-Singapore. Lighter shades denote the area bounded by the 10th and 90th percentiles, darker shades bound the 25th and 75th percentiles and the median is marked by a solid coloured line. Below each is a violin plot showing the average distribution for all heights, with the median, and 10th, 25th, 75th and 90th percentiles indicated. The median differences and standard deviations are, for (a) -0.44 ms^{-1} and 9.37 ms^{-1}, for (b) 0.15 ms^{-1} and 7.62 ms^{-1}, and for (c) 0.00 ms^{-1} and 3.37 ms^{-1}.

https://doi.org/10.5194/egusphere-2023-285
Preprint. Discussion started: 7 March 2023
© Author(s) 2023. CC BY 4.0 License.

and ERA5 respectively. The standard deviation across all heights is in broad agreement with existing literature (e.g. Rennie et al. (2021), Martin et al. (2021) and Lux et al. (2022)), although is slightly at the upper end of some estimates, with an average Aeolus-ERA5 difference of 7.62ms^{-1}.

In all three comparisons, there is greater spread between the datasets at higher altitudes, which corresponds with Aeolus' reducing SNR with height and the well known issue of less representative reanalysis winds in the stratosphere compared with the troposphere (Baldwin and Gray, 2005; Kawatani et al., 2016; Sivan et al., 2021). The reason for the lower Aeolus SNR above the tropopause is simply the reduced Rayleigh backscattering caused by atmospheric density dropping exponentially with altitude (Reitebuch et al., 2020), and is a feature seen in pre-launch simulations of Aeolus winds (Rennie, 2018). The Aeolus winds are generally easterly-biased relative to radiosonde measurements above the mid-troposphere, reaching a maximal bias of around -3 ms^{-1} near the tropopause itself, which is where the greatest differences tend to be for all three dataset comparisons. The bias becomes positive over the height range 10-12 km, but is largely negligible below this height. Throughout the main depth of the atmospheric profile, the standard deviation remains largely constant at around 8-9 ms^{-1}.

The most notable feature which stands out for both observing instruments relative to the reanalysis (figures 4b, c) is the significant easterly wind difference around the tropopause, with both Aeolus and the Singapore radiosonde profiles exhibiting a pronounced, yet relatively shallow deviation centered around 17 km. It is known from previous work that atmospheric reanalyses have historically shown a peak in bias around the tropopause. For example, the presence of a CPT warm bias in NCEP-NCAR (R1) is discussed by Tegtmeier et al. (2020) as being primarily due to the vertical resolution of the model. Notably, in the tropics this is related to Kelvin wave activity, and likely results from the use of poorly resolved satellite temperature retrievals, as explored by Fujiwara et al. (2017). The most likely cause of temperature biases at the tropopause is the smoothing of sharp vertical temperature gradients in the data assimilation system, with studies such as Flannaghan and Fueglistaler (2011, 2014) identifying a strong sensitivity in atmospheric reanalyses to mixing from shear-flow instabilities in connection with Kelvin waves. Wind data from Aeolus has been shown to contribute the highest changes in NWP skill around the tropical tropopause height, so it is suggested that this particular wind bias in the observing instruments seen in figure 4 is a consequence of the same issue related to vertical resolution and the failure of atmospheric reanalyses to accurately capture mixing due to Kelvin waves, as outlined above. In the context of the QBO disruption, which appears to have propagated upwards from the TTL region, the addition of Aeolus information both on its own and assimilated into future reanalyses is therefore likely to be very useful.

Another difference between Aeolus and ERA5 can be observed by comparing the timeseries of the QBO disruption in the zonal-mean HLOS wind for both simultaneously. Figure 5 shows that there is great similarity between the two datasets when a like-for-like comparison is made, however there are still some notable differences. In particular, the onset of the easterly winds at 22 km which characterises the disruption itself is delayed in the reanalysis by 5 days with respect to Aeolus. This lag appears to persist in time and is seen again with the onset of the -5 ms^{-1} isotach during January 2020.

The reason for this inconsistency in the disruption onset time is unclear, especially given that both ascending and descending node measurements are included in each daily wind calculation, thus ruling out any point-by-point systematic biases in either dataset as being the cause. The most likely cause is that the reanalysis' tendency to revert to its model climatology inhibits its

https://doi.org/10.5194/egusphere-2023-285
Preprint. Discussion started: 7 March 2023
© Author(s) 2023. CC BY 4.0 License.

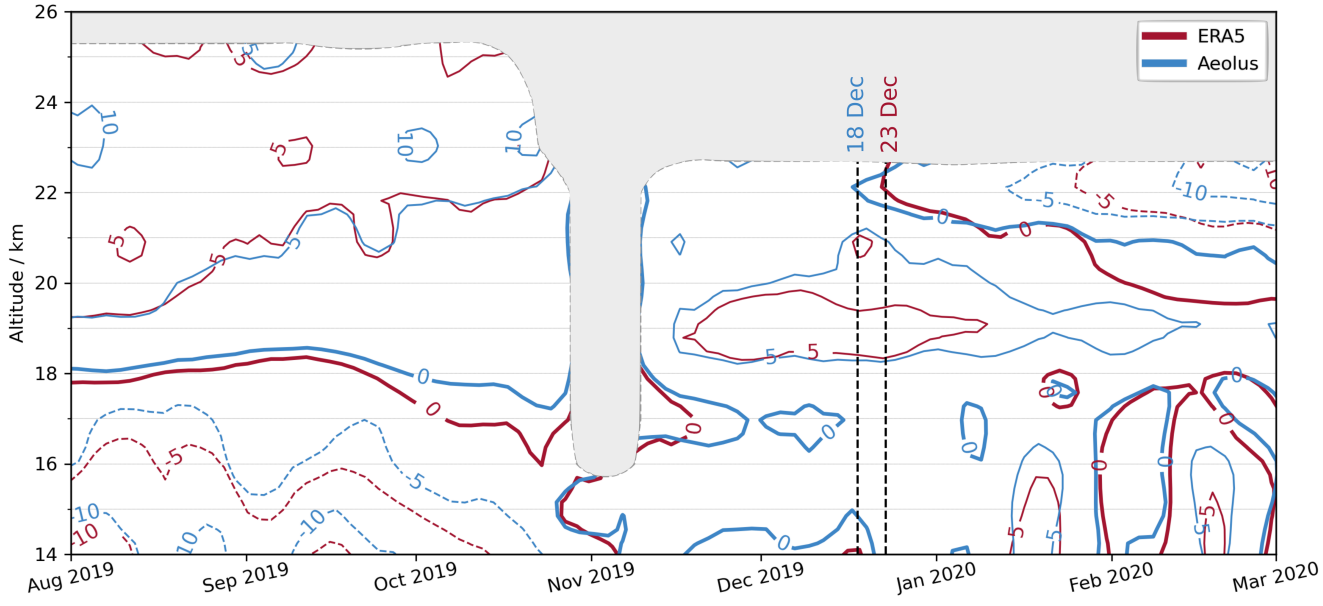

Figure 5. Timeseries of daily zonal-mean HLOS wind between 5°S - 5°N as in figure 1, but using coloured contours to show both Aeolus (blue) and ERA5 (red), and for the period August 2019 - March 2020. The dashed black vertical lines mark the time of the onset of easterly winds at 22 km for Aeolus and ERA5, as 18 December 2019 and 23 December 2019 respectively.

ability to match the progress of the disruption as measured using observations, including Aeolus. By definition, the disruption itself is an anomalous feature in the tropical lower stratosphere relative to climatology. Additionally, the zonally inhomogeneous sampling of wind measurements assimilated into the reanalysis means that data from certain locations may bias the zonal-mean wind calculation made here. Conversely, Aeolus is measuring across all longitudes with a near-homogeneous repeating orbital pattern, so the zonal-mean should be less affected by regional wind biases.

3.3 Equatorial waves during the QBO disruption

Figure 6 shows time-filtered Hövmoller diagrams (where time is placed on the y axis) of the eddy zonal wind (i.e. $u' = u - \overline{u}$) for both Aeolus and ERA5 at an altitude of 16 km, with the difference between the two in the centre panel. Figure S1 in the supplementary material shows the raw, unfiltered winds for completeness. As a result of filtering with a Gaussian band-pass filter to highlight only wind structures with a period of 5-25 days, Kelvin wave activity can be seen with varying intensity for the duration of the disruption, in both Aeolus and ERA5. Although these waves are notably slower than typical Kelvin wave periods (7-10 days) such as those analysed in OLR data from NOAA polar orbiting satellites by Wheeler and Kiladis (1999), some observational studies identify three discrete frequency regimes for Kelvin waves, including so-called "Wallace-Kousky" or "slow" waves, with periods of order 10-20 days (Wallace and Kousky, 1968; Canziani et al., 1994; Forbes et al.,

https://doi.org/10.5194/egusphere-2023-285
Preprint. Discussion started: 7 March 2023
© Author(s) 2023. CC BY 4.0 License.

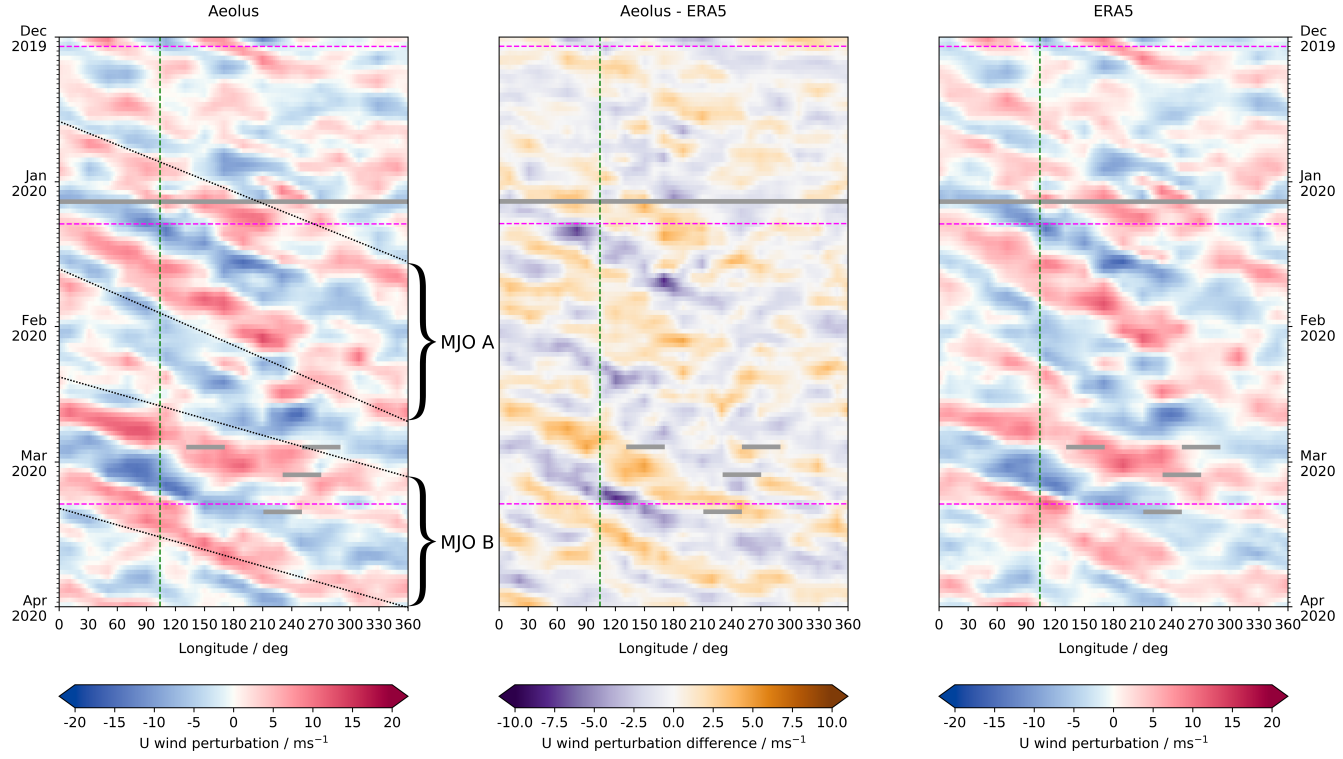

Figure 6. Time-filtered Hövmoller plots of zonal wind perturbations from the zonal-mean at 16 km for the December 2019 - April 2020 disruption time period, for (a) Aeolus, (c) ERA5 as Aeolus and (b) the difference between (a) and (c). The 3 dashed magenta lines during the period of the disruption correspond to the cross-sectional snapshots in figure 7. The vertical dashed green lines mark the longitude of the Singapore radiosonde launch site, 104°. Data is interpolated onto a 2° resolution longitude grid to enable the wave progression to be seen more clearly.

2009). Furthermore, another study, Shimizu and Tsuda (1997), carried out a periodogram analysis of a radiosonde campaign in Indonesia and found a dominant Kelvin wave period of 20-25 days in the 15-20 km altitude range, which agrees well with the results here.

Another possible explanation for the slower speed of these waves are the "superclusters" noted by Nakazawa (1988) and Dunkerton and Crum (1995) amongst others; indeed, the former study identifies several smaller clusters of convective activity which propagate embedded within a larger tropical intraseasonal oscillation (TIO), while the latter alludes to anomalies with periods up to 15 days traversing within a TIO with period 30-60 days. Such a long-period oscillation is today termed the Madden-Julian Oscillation (MJO), and it is likely that the two larger-scale pulses in amplitude seen in figure 6 form the active phases of the MJO (marked 'MJO A' and 'MJO B'), within which these eastward propagating Kelvin waves can be seen. Kikuchi et al. (2018) examines the relationship between the MJO and such counter-clockwise equatorial waves (CCEW) and

https://doi.org/10.5194/egusphere-2023-285
Preprint. Discussion started: 7 March 2023
© Author(s) 2023. CC BY 4.0 License.

proposes in a similar way that Kelvin waves can act almost as building blocks for the larger MJO envelope, a picture that matches the phase progression of the waves in this figure.

In figure 6b the difference between Aeolus and ERA5 can be seen, showing relatively small differences maximising around 5-10 ms^{-1}, which is in line with expectations from the random error between the two datasets observed earlier. Aeolus winds are generally stronger than ERA5 winds in each zonal wind pulse, consistent with a pattern that exhibits the same Kelvin wave behaviour; and typically the timing of each phase in Aeolus slightly precedes the same in ERA5.

This analysis shows that whilst perhaps weaker than in the case of the 2015-16 disruption, as alluded to by Kang and Chun (2021), much Kelvin wave activity during the mature phase of the 2019-20 disruption is still easily observable by Aeolus. The vertical bursts of westerly winds seen in the zonal mean in the UTLS in figure 1 appear to correspond to two larger-scale pulses which themselves are comprised of smaller-scale eastward propagating Kelvin waves. This is despite the theoretical assumption that Kelvin waves register no signal in the zonal-mean; suggesting that real observations can still produce some small signature, potentially due to land/ocean variability.

Figure 7 shows three vertical along-equator cross-sections of the eddy zonal wind for Aeolus. For ease of comparison with the wind profiles at Singapore in figure 3, the green dashed lines demarcate the longitude of the Singapore radiosonde launches and co-located Aeolus and ERA5 profiles. Each cross-section corresponds to the dashed magenta lines seen in both figure 1 and figure 4. These dates are chosen firstly to represent an even temporal spread across the QBO disruption, secondly to match the snapshots in figure 3 as closely as possible, and thirdly yet most importantly, since the vertical structure of an equatorial Kelvin wave can be seen in each of them.

In all three cross-sections, there is a strong dipole in zonal wind centered around 180° longitude, likely corresponding to divergence associated with the upwelling maximum of the Walker Circulation in the west Pacific ocean. This feature can also be seen in figure S1 and animation S2 in the supplementary material, with a dipole centred around the same longitude. Upper-level horizontal divergence is at a maximum here, and remains as a quasi-stationary feature in similar cross-sections during this period (not shown). To the west of this, the diagonally slanted pattern of a Kelvin wave can be seen, maximising in amplitude around the longitude of the maritime continent, between ∼(95-155)°E.

The fine vertical resolution offered by Aeolus shows a strong vertical gradient in the zonal wind around the tropopause where the Kelvin wave amplitude is greatest, particularly in figure 7b and c. Easterly winds associated with the westward branch of the Walker Circulation are overlaid by westerly winds above, which traverse swiftly eastward in time (not shown), in correspondence with the Hövmoller plot in figure 6.

The wave-like structure of the wind profile between 15-22 km at the longitude of Singapore in the first cross-section (figure 7a) matches the corresponding profile a day later in figure 3d very well. The general morphology of this snapshot is similar to the following two cross-sections, but the Kelvin wave amplitude is weaker, matching the same behaviour seen in figure 6. The data here is interpolated onto a finer grid in longitude which enables the wave to be seen more clearly, however the coarseness of the original data is still visible. This coarseness is caused by the horizontal spacing between each Aeolus overpass in the tropics, such that with 16 complete orbits there are 32 individual overpasses each day (ascending and descending nodes), separated by an average of around 12° longitude. As a consequence, Aeolus' analysis of equatorial waves in the tropics is

https://doi.org/10.5194/egusphere-2023-285
Preprint. Discussion started: 7 March 2023
© Author(s) 2023. CC BY 4.0 License.

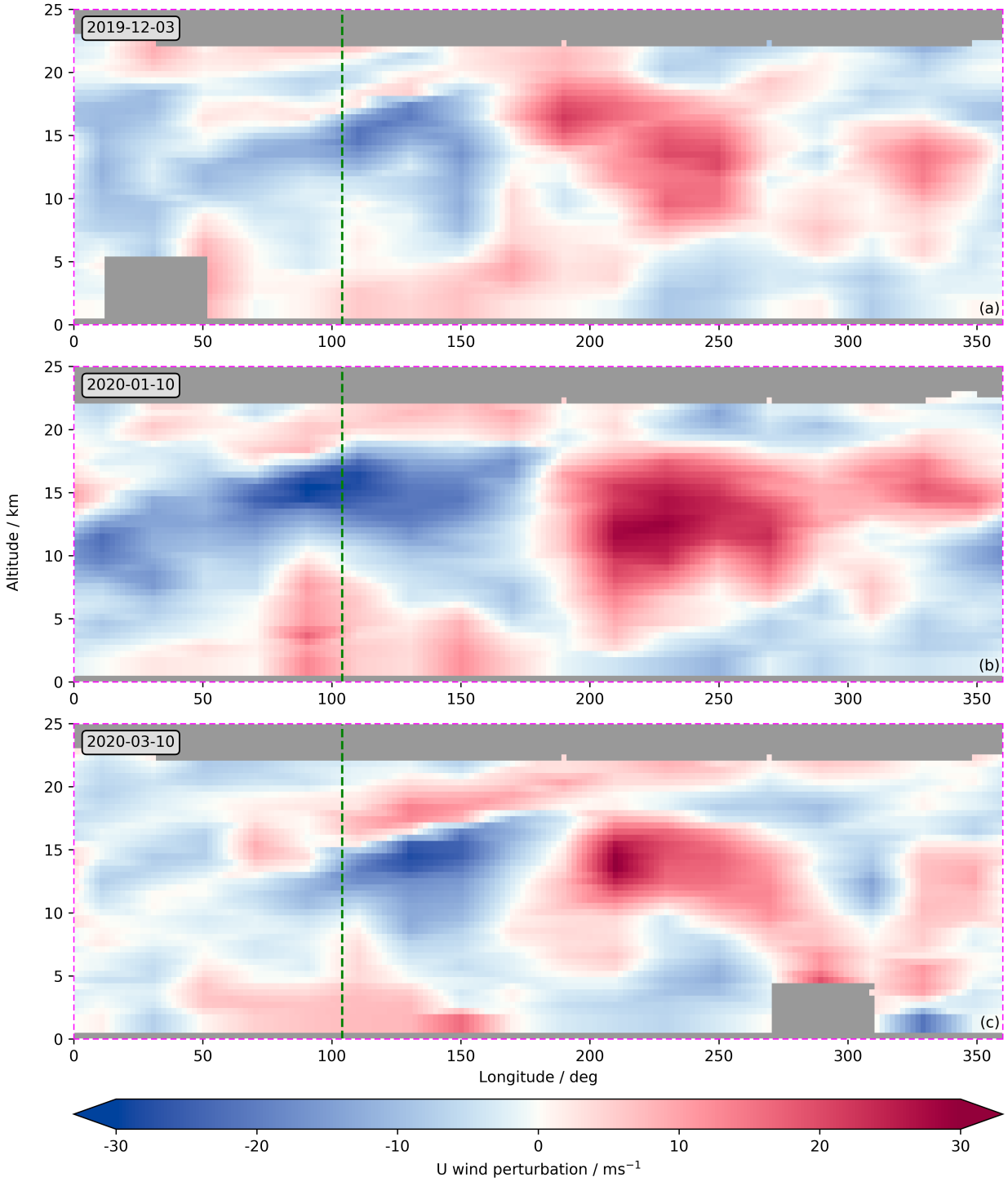

Figure 7. Vertical along-equator cross-sections of the daily averaged zonal wind perturbation from the zonal-mean between 5°N and 5°S for (a) 2019-12-03, (b) 2020-01-10, and (c) 2020-03-10. Data is interpolated onto a 2° resolution longitude grid to enable the Kelvin wave structure to be seen more clearly. The vertical dashed green line marks the longitude of the Singapore radiosonde launch site, 104°, as in figure 6.

https://doi.org/10.5194/egusphere-2023-285
Preprint. Discussion started: 7 March 2023
© Author(s) 2023. CC BY 4.0 License.

limited by this constraint, which could prove a challenge if attempting to investigate smaller-scale features involved in the dynamics of the QBO disruption.

4 Discussion

Overall, the primary limitation on observing the QBO disruption using Aeolus is the limited vertical extent of the measurements, due to the height range covered by the onboard range-bin settings during this period. Since Aeolus is a demonstration Earth Explorer mission, these settings change regularly in response to calibration/validation analysis, evolving NWP requirements and multiple scientific campaigns aimed at the development of a future operational wind lidar platform. Aeolus' designed maximum measurement altitude is 30 km, which was briefly reached during a short period in early 2022 whilst observing the impacts of the Hunga Tonga volcano eruption. Given that much of the QBO's progression occurs in the 20 - 30 km range, any future space-borne wind lidar that operationally measures winds at these heights with the same measurement geometry as Aeolus will capture a greater depth of the QBO and for a longer time period. Nonetheless, the weekly QBO 2020 RBS that were introduced in June 2019 contributed significantly to observations of the lower portion of the QBO after this date.

Another limitation of the Aeolus data is in the persistent random error with respect to both the Singapore radiosonde and ERA5 reanalysis, of 9.37 ms^{-1} and 7.62 ms^{-1} respectively for the profiles in figure 3. This random error has been shown by Lux et al. (2022) to increase gradually over the time duration of the FM-B laser portion of the mission, in line with a gradual decrease in the return energy from each laser pulse from the ALADIN instrument. Although for some purposes this random error poses less of an issue, such as case studies covering less than a day, and studies involving calculations of wind perturbations (e.g. Banyard et al. (2021)), when looking at raw winds in the UTLS this error component could pose a bigger problem. Here, the QBO disruption is analysed over the entire period firstly in a zonal-mean framework, where the averaging of many measurements lends more confidence in the accuracy of the final result. The time-varying random error will however have a greater impact on the results from the validation exercise with comparisons to radiosonde and reanalysis data, since although they cover a shorter time frame, the ALADIN instrument did still experience some minor fluctuations in energy output during this period.

In addition to the constraints provided by the data's vertical extent and associated random errors, Aeolus also presents limitations in the horizontal plane. In order to study equatorial wave activity during the disruption, and in particular the role of Kelvin waves, the eddy component of the zonal wind has to be isolated from the zonal-mean zonal wind, and analysed as a function of longitude. Given the average separation of Aeolus orbits in the tropics is around 12°, the longitudinal resolution of Aeolus data limits this analysis. Through either the careful averaging of data to suit a study's specific requirements, or the assimilation of data into a reanalysis model, this issue can be overcome.

Since the Aeolus mission was launched in 2018 it has provided measurements for a limited time-frame of around 4 years, and the onboard settings have been tuned to observe the QBO for just a portion of this. Given the long oscillation period of the QBO, and since much of the Aeolus measurement time-frame is dominated by the disruption of 2019-20, it is difficult to use Aeolus data to study the normal progression of this phenomena, and in particular to answer questions relating to the occurrence

https://doi.org/10.5194/egusphere-2023-285
Preprint. Discussion started: 7 March 2023
© Author(s) 2023. CC BY 4.0 License.

of QBO disruptions in the future. Some global climate models infer an increased frequency of disruptions as a consequence of climate change (Anstey et al., 2021), however with just two such disruptions so far there is a limited sample size of events to study. It may be that disruptions either are or have become part of the natural cycle of the QBO on longer timescales. Kang et al. (2022) suggests that stronger westerly winds in the equatorial lower stratosphere as a consequence of climate change will provide more favourable conditions for QBO disruptions in the future. Although the limited time duration of the Aeolus mission prevents this question from being answered here, future operational Doppler wind lidar (DWL) satellites that measure tropical stratospheric winds will be better able to observe such changes.

5 Conclusions

In conclusion, this study has investigated the 2019/2020 QBO disruption using novel data from ESA's Aeolus satellite. Aeolus is very well suited to observing zonal wind phenomena in the tropics because of its measurement geometry. It can observe the lower portion of the QBO, and with changes to the onboard range-bin settings made in 2020, can see much more of the QBO's phase progression in the lower stratosphere. The evolution of the disruption with the anomalous upward propagating easterly jet and overlying westerly winds can be seen using Aeolus, although this is hindered slightly by the satellite's vertical measurement range at the time. The maximum zonal-mean easterly winds within the part of the disruption jet that can be observed by Aeolus reaches 20 ms^{-1} during July 2020. Aeolus then captures the following downward propagating westerly QBO phase, followed by the next easterly QBO phase at high altitudes, which is aided by settings to observe wind returns from high-altitude aerosol resulting from the Hunga Tonga eruption in January 2022.

There is good agreement between co-located profiles using Aeolus, Singapore radiosonde and ERA5 data, although there exists a small negative wind bias near the tropopause which is likely a result of insufficient vertical resolution as well as deficits in the data assimilation of existing satellite data in the reanalysis. The standard deviation of the differences between the datasets is in broad agreement with existing literature, with an average Aeolus-ERA5 difference of 7.62ms^{-1}, although there is greater spread at higher altitudes due to the decreasing Aeolus SNR here. The onset of the easterly disruption anomaly at 22 km occurs on 18 December 2019 in the Aeolus zonal-mean HLOS wind, preceding the wind reversal in ERA5 by 5 days. This is most likely to be caused by the renalysis' tendency to revert to its model climatology, which will not adequately reflect the dynamics of the disruption.

During the disruption, Aeolus captures slow eastward-propagating Kelvin waves, embedded within larger clusters of westerly zonal wind pulses which are likely associated with the active phase of the MJO. In agreement with the data validation, Aeolus winds are generally stronger than ERA5 in each wave pulse, and the phase precedes that of the reanalysis slightly. The structural morphology of the Kelvin waves can be seen in a vertical along-equator cross-section of the zonal wind, which shows diagonally oriented wave fronts and a maximum wave amplitude near the maritime continent. This analysis also showed the key features of the Walker Circulation with a dipole in zonal wind centred on the west Pacific Ocean.

Finally, some of the limitations of using Aeolus data to analyse the QBO disruption and the dynamics of the tropical stratosphere more generally have been explored. The primary constraint is the limited vertical extent of the measurements due to the

https://doi.org/10.5194/egusphere-2023-285
Preprint. Discussion started: 7 March 2023
© Author(s) 2023. CC BY 4.0 License.

onboard range-bin settings during the period of analysis. However, the random error of Aeolus winds and reduced longitudinal resolution caused by orbital geometry also play a key role in adding uncertainty to the results. In spite of these, Aeolus and future DWL satellites show a lot of promise in observing events like the 2019-20 QBO disruption, and their contribution to future reanalyses is likely to improve our understanding of the mechanisms behind such events even further.

Author contributions. TPB - Conceptualization, Data curation, Formal Analysis, Investigation, Methodology, Project administration, Software, Validation, Visualization, Writing – original draft, Writing – review & editing.

CJW - Conceptualization, Data curation, Funding acquisition, Investigation, Methodology, Project administration, Resources, Software, Supervision, Writing – original draft, Writing – review & editing.

SMO - Conceptualization, Methodology, Writing – review & editing.

NPH - Conceptualization, Methodology, Software, Supervision, Validation, Writing – review & editing.

GH - Conceptualization, Writing – review & editing.

LC - Conceptualization, Writing – review & editing.

PAN - Conceptualization, Writing – review & editing.

NB - Conceptualization, Writing – review & editing.

Competing interests. The authors declare that they have no competing interests.

Acknowledgements. The authors would like to thank the Aeolus DISC team for supporting this study and for their helpful communications throughout. T. P. Banyard is funded by Royal Society grant RGF/EA/180217 and EPSRC grant EP/R513155/1. C. J. Wright is funded by Royal Society grant RF/ERE/210079 and NERC grant NE/V01837X/1. C. J. Wright and N. P. Hindley are funded by NERC grant NE/R001391/1 and NE/S00985X/1.

https://doi.org/10.5194/egusphere-2023-285
Preprint. Discussion started: 7 March 2023
© Author(s) 2023. CC BY 4.0 License.

References

Abdalla, S., Aprile, S., Mellano, L., De Laurentis, M., Fischer, P., Von Bismarck, J., Krisch, I., Reitebuch, O., Masoumzadeh, N., Flament, T., Trapon, D., Weiler, F., Bucci, S., Gostinicchi, G., De Kloe, J., Rennie, M., and Isaksen, L.: Aeolus: First FM-B science data reprocessing campaign, Aeolus CAL/VAL and Science Workshop 2020, 2020.

Angell, J. K. and Korshover, J.: Quasi-Biennial Variations in Temperature, Total Ozone, and Tropopause Height, Journal of the Atmospheric Sciences, 21, 479–492, https://doi.org/10.1175/1520-0469(1964)021<0479:QBVITT>2.0.CO;2, 1964.

Anstey, J., Banyard, T., Butchart, N., Coy, L., Newman, P., Osprey, S., and Wright, C.: Prospect of increased disruption to the QBO in a changing climate., Geophysical Research Letters, https://doi.org/10.1029/2021GL093058, 2021.

Baldwin, M. and Gray, L.: Tropical stratospheric zonal winds in ECMWF ERA-40 reanalysis, rocketsonde data, and rawinsonde data, Geophysical Research Letters, 32, https://doi.org/10.1029/2004GL022328, 2005.

Banyard, T., Wright, C., Hindley, N., Halloran, G., Krisch, I., Kaifler, B., and Hoffmann, L.: Atmospheric gravity waves in Aeolus wind lidar observations., Geophysical Research Letters, https://doi.org/10.1029/2021GL092756, 2021.

Barton, C. A. and McCormack, J. P.: Origin of the 2016 QBO Disruption and Its Relationship to Extreme El Niño Events, Geophysical Research Letters, 44, 11,150–11,157, https://doi.org/10.1002/2017GL075576, 2017.

Bushell, A., Anstey, J., Butchart, N., Kawatani, Y., Osprey, S., Richter, J., Serva, F., Braesicke, P., Cagnazzo, C., Chen, C., and Chun, H.: Evaluation of the Quasi-Biennial Oscillation in global climate models for the SPARC QBO-initiative., Quarterly Journal of the Royal Meteorological Society, https://doi.org/10.1002/qj.3765, 2020.

Canziani, P., Holton, J., Fishbein, E., Froidevaux, L., and Waters, J.: Equatorial Kelvin waves: a UARS MLS view., Journal of the Atmospheric Sciences, 51, 3053–3076, https://doi.org/10.1175/1520-0469(1994)051<3053:EKWAUM>2.0.CO;2, 1994.

Chanin, M., Garnier, A., Hauchecorne, A., and Porteneuve, J.: A Doppler lidar for measuring winds in the middle atmosphere., Geophysical Research Letters, 16, https://doi.org/10.1029/GL016i011p01273, 1989.

Chen, H.-C., Tseng, Y.-H., Hu, Z.-Z., and Ding, R.: Enhancing the ENSO Predictability beyond the Spring Barrier, Scientific Reports, 10, 1–12, https://doi.org/10.1038/s41598-020-57853-7, 2020.

Coy, L., Newman, P. A., Pawson, S., and Lait, L. R.: Dynamics of the Disrupted 2015/16 Quasi-Biennial Oscillation, Journal of Climate, 30, 5661–5674, https://doi.org/10.1175/JCLI-D-16-0663.1, 2017.

Dunkerton, T. J. and Crum, F. X.: Eastward propagating ∼2- to 15-day equatorial convection and its relation to the tropical intraseasonal oscillation, Journal of Geophysical Research: Atmospheres, 100, 25 781–25 790, https://doi.org/10.1029/95JD02678, 1995.

Durre, I., Yin, X., Vose, R., Applequist, S., and Arnfield, J.: Enhancing the data coverage in the Integrated Global Radiosonde Archive., Journal of Atmospheric and Oceanic Technology, 35, 1753–1770, https://doi.org/10.1175/JTECH-D-17-0223.1, 2018.

ESA: ALADIN - Atmospheric Laser Doppler Instrument. Working Group Report, ESA SP-1112, p. 45p, 1989.

ESA: ADM-Aeolus Science Report, ESA SP-1311, p. 121p, 2008.

Feng, P. N. and Lin, H.: Modulation of the MJO-Related Teleconnections by the QBO, Journal of Geophysical Research: Atmospheres, 124, https://doi.org/10.1029/2019JD030878, 2019.

Flannaghan, T. J. and Fueglistaler, S.: Kelvin waves and shear-flow turbulent mixing in the TTL in (re-)analysis data., Geophysical Research Letters, 38, https://doi.org/10.1029/2010GL045524, 2011.

Flannaghan, T. J. and Fueglistaler, S.: Vertical Mixing and the Temperature and Wind Structure of the Tropical Tropopause Layer, Journal of Atmospheric Sciences, 71, 1609–1622, https://doi.org/10.1175/JAS-D-13-0321.1, 2014.

https://doi.org/10.5194/egusphere-2023-285
Preprint. Discussion started: 7 March 2023
© Author(s) 2023. CC BY 4.0 License.

Forbes, J., Zhang, X., Palo, S., Russell, J., Mertens, C., and Mlynczak, M.: Kelvin waves in stratosphere, mesosphere and lower thermosphere temperatures as observed by TIMED/SABER during 2002–2006., Earth, planets and space, 61, 447–453, https://doi.org/10.1186/BF03353161, 2009.

Fujiwara, M., Wright, J. S., Manney, G. L., Gray, L. J., Anstey, J., Birner, T., Davis, S., Gerber, E. P., Harvey, V. L., Hegglin, M. I., and Homeyer, C. R.: Introduction to the SPARC Reanalysis Intercomparison Project (S-RIP) and overview of the reanalysis systems., Atmospheric Chemistry and Physics, 17, 1417–1452, https://doi.org/10.5194/acp-17-1417-2017, 2017.

Hersbach, H., Bell, B., Berrisford, P., Hirahara, S., Horányi, A., Muñoz-Sabater, J., Nicolas, J., Peubey, C., Radu, R., Schepers, D., and Simmons, A.: The ERA5 global reanalysis., Quarterly Journal of the Royal Meteorological Society, 146, 1999–2049, https://doi.org/10.1002/qj.3803, 2020.

Highwood, E. J. and Hoskins, B. J.: The Tropical Tropopause, Quarterly Journal of the Royal Meteorological Society, 124, 1579–1604, https://doi.org/10.1002/qj.49712454911, 1998.

Kang, M. and Chun, H.: Contributions of equatorial waves and small-scale convective gravity waves to the 2019/20 quasi-biennial oscillation (QBO) disruption., Atmospheric Chemistry and Physics, 21, https://doi.org/10.5194/acp-21-9839-2021, 2021.

Kang, M., Chun, H., and Garcia, R. R.: Role of equatorial waves and convective gravity waves in the 2015/16 quasi-biennial oscillation disruption, Atmospheric Chemistry and Physics, 20, https://doi.org/10.5194/acp-20-14669-2020, 2020.

Kang, M., Chun, H., Son, S., Garcia, R., An, S., and Park, S.: Role of tropical lower stratosphere winds in quasi-biennial oscillation disruptions, Science Advances, 8, https://doi.org/10.1126/sciadv.abm7229, 2022.

Kawatani, Y., Hamilton, K., Miyazaki, K., Fujiwara, M., and Anstey, J.: Representation of the tropical stratospheric zonal wind in global atmospheric reanalyses., Atmospheric Chemistry and Physics, 16, 6681–6699, https://doi.org/10.5194/acp-16-6681-2016, 2016.

Kikuchi, K., Kiladis, G. N., Dias, J., and Nasuno, T.: Convectively coupled equatorial waves within the MJO during CINDY/DYNAMO: slow Kelvin waves as building blocks., Climate Dynamics, 50, 4211–4230, https://doi.org/10.1007/s00382-017-3869-5, 2018.

Krisch, I., Hindley, N. P., Reitebuch, O., and Wright, C. J.: On the derivation of zonal and meridional wind components from Aeolus horizontal line-of-sight wind, Atmospheric Measurement Techniques, 15, 3465–3479, https://doi.org/10.5194/amt-15-3465-2022, 2022.

Latif, M., Anderson, D., Barnett, T., Cane, M., Kleeman, R., Leetmaa, A., O'Brien, J., Rosati, A., and Schneider, E.: A review of the predictability and prediction of ENSO, Journal of Geophysical Research: Oceans, 103, 14 375–14 393, https://doi.org/10.1029/97JC03413, 1998.

Legras, B., Duchamp, C., Sellitto, P., Podglajen, A., Carboni, E., Siddans, R., Grooß, J. U., Khaykin, S., and Ploeger, F.: The evolution and dynamics of the Hunga Tonga–Hunga Ha'apai sulfate aerosol plume in the stratosphere., Atmospheric Chemistry and Physics, 22, 14 957–14 970, https://doi.org/10.5194/acp-22-14957-2022, 2022.

Lim, Y., Son, S. W., Marshall, A. G., Hendon, H. H., and Seo, K. H.: Influence of the QBO on MJO prediction skill in the subseasonal-to-seasonal prediction models, Climate Dynamics, 53, 1681–1695, https://doi.org/10.1007/s00382-019-04719-y, 2019.

Lux, O., Witschas, B., Geiß, A., Lemmerz, C., Weiler, F., Marksteiner, U., Rahm, S., Schäfler, A., and Reitebuch, O.: Quality control and error assessment of the Aeolus L2B wind results from the Joint Aeolus Tropical Atlantic Campaign., Atmospheric Measurement Techniques, 15, 6467–6488, https://doi.org/10.5194/amt-15-6467-2022, 2022.

Martin, A., Weissmann, M., Reitebuch, O., Rennie, M., Geiß, A., and Cress, A.: Validation of Aeolus winds using radiosonde observations and numerical weather prediction model equivalents., Atmospheric Measurement Techniques, 14, 2167–2183, https://doi.org/10.5194/amt-14-2167-2021, 2021.

https://doi.org/10.5194/egusphere-2023-285
Preprint. Discussion started: 7 March 2023
© Author(s) 2023. CC BY 4.0 License.

Nakazawa, T.: Tropical super clusters within intraseasonal variations over the western Pacific., Journal of the Meteorological Society of Japan. Ser. II, 66, 823–839, https://doi.org/10.2151/jmsj1965.66.6_823, 1988.

Naujokat, B.: An Update of the Observed Quasi-Biennial Oscillation of the Stratospheric Winds over the Tropics, Journal of the Atmospheric Sciences, 43, 1873–1877, https://doi.org/10.1175/1520-0469(1986)043<1873:AUOTOQ>2.0.CO;2, 1986.

Newman, P., Coy, L., Pawson, S., and Lait, L.: The anomalous change in the QBO in 2015– 2016., Geophysical Research Letters, https://doi.org/10.1002/2016GL070373, 2016.

Osprey, O. M., Butchart, N., Knight, J. R., Scaife, A. A., Hamilton, K., Anstey, J. A., Schenzinger, V., and Zhang, C.: An unexpected disruption of the atmospheric quasi-biennial oscillation, Science, pp. 1424–1427, https://doi.org/10.1126/science.aah4156, 2016.

Reed, R. J.: The present status of the 26-month oscillation, Bulletin of the American Meteorological Society, 46, 374–387, https://doi.org/10.1175/1520-0477-46.7.374, 1965.

Reid, G. C. and Gage, K. S.: Interannual variations in the height of the tropical tropopause, Journal of Geophysical Research: Atmospheres, 90, 5629–5635, https://doi.org/10.1029/JD090iD03p05629, 1985.

Reitebuch, O.: The spaceborne wind lidar mission ADM-Aeolus., Atmospheric Physics, pp. 815–827, https://doi.org/10.1007/978-3-642-30183-4_49, 2012.

Reitebuch, O., Lemmerz, C., Lux, O., Marksteiner, U., Rahm, S., Weiler, F., Witschas, B., Meringer, M., Schmidt, K., Huber, D., Nikolaus, I., Geiss, A., Vaughan, M., Dabas, A., Flament, T., Stieglitz, H., Isaksen, L., Rennie, M., de Kloe, J., Marseille, G., Stoffelen, A., Wernham, D., Kanitz, T., Straume, A., Fehr, T., von Bismarck, J., Floberghagen, R., and Parrinello, T.: Initial Assessment of the Performance of the First Wind Lidar in Space on Aeolus., EPJ Web of Conferences, 237, https://doi.org/10.1051/epjconf/202023701010, 2020.

Rennie, M.: An assessment of the expected quality of Aeolus Level-2B wind products, EPJ Web of Conferences, 176, https://doi.org/10.1051/epjconf/201817602015, 2018.

Rennie, M. P., Isaksen, L., Weiler, F., de Kloe, J., Kanitz, T., and Reitebuch, O.: The impact of Aeolus wind retrievals on ECMWF global weather forecasts., Quarterly Journal of the Royal Meteorological Society, 147, 3555–3586, https://doi.org/10.1002/qj.4142, 2021.

Scaife, A. A., Athanassiadou, M., Andrews, M., Arribas, A., Baldwin, M., Dunston, N., Knight, J., MacLachlan, C., Manzini, E., Müller, W. A., Pohlmann, H., Smith, D., Stockdale, T., and Williams, A.: Predictability of the quasi-biennial oscillation and its northern winter teleconnection on seasonal to decadal timescales, Geophysical Research Letters, 41, 1752–1758, https://doi.org/10.1002/2013GL059160, 2014.

Seiki, A. and Takayabu, Y. N.: Westerly Wind Bursts and Their Relationship with Intraseasonal Variations and ENSO. Part I: Statistics., Monthly Weather Review, 135, 3325–3345, https://doi.org/10.1175/MWR3477.1, 2007.

Shimizu, A. and Tsuda, T.: Characteristics of Kelvin waves and gravity waves observed with radiosondes over Indonesia., Journal of Geophysical Research: Atmospheres, 102, 26 159–26 171, https://doi.org/10.1029/96JD03146, 1997.

Sivan, C., Rakesh, V., Abhilash, S., and Mohanakumar, K.: Evaluation of global reanalysis winds and high-resolution regional model outputs with the 205 MHz stratosphere–troposphere wind profiler radar observations, Quarterly Journal of the Royal Meteorological Society, https://doi.org/10.1002/qj.4041, 2021.

Stoffelen, A., Pailleux, J., Källén, E., Vaughan, J., Isaksen, L., Flamant, P., Wergen, W., Andersson, E., Schyberg, H., Culoma, A., and Meynart, R.: The atmospheric dynamics mission for global wind field measurement., Bulletin of the American Meteorological Society, 86, https://doi.org/10.1175/BAMS-86-1-73, 2005.

Tan, X., Tang, Y., Lian, T., Yao, Z., Li, X., and Chen, D.: A study of the effects of westerly wind bursts on ENSO based on CESM, Climate Dynamics, 54, 885–899, https://doi.org/10.1007/s00382-019-05034-2, 2020.

https://doi.org/10.5194/egusphere-2023-285
Preprint. Discussion started: 7 March 2023
© Author(s) 2023. CC BY 4.0 License.

Tegtmeier, S., Anstey, J., Davis, S., Ivanciu, I., Jia, Y., McPhee, D., and Kedzierski, R. P.: Zonal Asymmetry of the QBO Temperature Signal in the Tropical Tropopause Region, Geophysical Research Letters, 47, https://doi.org/10.1029/2020GL089533, 2020.

Vaisala: Comparison of Vaisala Radiosondes RS41 and RS92: Ref. B211317EN-B, p. 14, https://www.vaisala.com/sites/default/files/documents/RS-Comparison-White-Paper-B211317EN.pdf, Accessed: 2021-07-28, 2014.

Wallace, J. M.: General circulation of the tropical lower stratosphere, Reviews of Geophysics, 11, 191–222, https://doi.org/10.1029/RG011i002p00191, 1973.

Wallace, J. M. and Kousky, V. E.: Observational Evidence of Kelvin Waves in the Tropical Stratosphere., Journal of the Atmospheric Sciences, 25, 900–907, https://doi.org/10.1175/1520-0469(1968)025<0900:OEOKWI>2.0.CO;2, 1968.

Weiler, F., Rennie, M., Kanitz, T., Isaksen, L., Checa, E., de Kloe, J., Okunde, N., and Reitebuch, O.: Correction of wind bias for the lidar on board Aeolus using telescope temperatures., Atmospheric Measurement Techniques, 14, 7167–7185, https://doi.org/10.5194/amt-14-7167-2021, 2021.

Wheeler, M. and Kiladis, G.: Convectively coupled equatorial waves: Analysis of clouds and temperature in the wavenumber–frequency domain., Journal of the Atmospheric Sciences, 56, 374–399, https://doi.org/10.1175/1520-0469(1999)056<0374:CCEWAO>2.0.CO;2, 1999.

Zheng, F. and Zhu, J.: Spring predictability barrier of ENSO events from the perspective of an ensemble prediction system, Global and Planetary Change, 72, 108–117, https://doi.org/10.1016/j.gloplacha.2010.01.021, 2010.